Effects of grain models on UV penetration into clouds

Chlewicki, G.; Greenberg, J.M.

Mon. Not. R. astr. Soc. (1984) **211**, 719–736

Effects of grain models on UV penetration into clouds

Grzegorz Chlewicki* and J. Mayo Greenberg
Astrophysics Laboratory, Huygens Laboratory, PO Box 9504, 2300 RA, Leiden, The Netherlands

Accepted 1984 July 2. Received 1984 June 25; in original form 1984 April 13

Summary. A derivation of the average scattering characteristics of interstellar grains in the ultraviolet based mainly on observations of extinction is shown to be more reliable than a determination from direct measures of scattered light. Several representative scattering models are constructed and their consequences for the transfer of UV radiation in clouds are discussed using the spherical harmonic expansion method (Flannery, Roberge & Rybicki 1980). Because of the presence of large grains ($a \sim 0.15\ \mu$m) in the size distribution, all models are characterized by strongly anisotropic scattering throughout the UV ($g \approx 0.7-0.9$) with a relatively low albedo ($\alpha < 0.4$ for $\lambda < 2500$ Å) resulting from the presence of very small grains ($a \leqslant 0.01\ \mu$m). An approximate algorithm replacing the exact solution of the radiative transfer equation by a greatly simplified solution for $g = 1$ is presented. It is shown to be accurate to within < 10 per cent at low and intermediate optical depths ($\tau < 20$) for $g > 0.7$ and $\alpha < 0.4$ and to give a deviation of less than a factor of 2 for g as low as $g = 0.5$.

1 Introduction

The amount of UV radiation in clouds is one of the crucial quantities determining their physical and chemical evolution. For clouds with no internal sources of energy, the UV light penetrating from outside is the only source of photons which is powerful enough to influence significantly the physical processes within the cloud. The next most important source of energy, the H_2 luminescence caused by cosmic rays, can only produce, even in relatively dense clouds, photon fluxes 10^4-10^5 times weaker than the general diffuse background outside (Prasad & Tarafdar 1983). Therefore, at low optical depths where the amount of UV light is high enough to play an important role, photons penetrating into the cloud dominate the radiation field and determine the characteristics of the cloud.

The scattering of UV photons by interstellar grains results from a superposition of scattering by at least two grain populations each of which is made up of grains of different

* Currently on leave of absence from N. Copernicus University, Torun, Poland.

sizes and with inhomogeneous properties. An approximation to the transfer of UV radiation for this complex system can be reasonably well described in terms of two basic parameters: the average albedo, α, and the average asymmetry factor, g. Since UV observations became possible, several attempts have been made to measure α and g from direct observations of UV light scattered by grains. In the next section we shall demonstrate that this approach is so burdened with difficulties and uncertainties that it leads almost inevitably to confusing and inconsistent results. The main purpose of this paper is to propose an alternative to the direct observational determination of α and g by calculating them from approximate models of grain populations. The observational basis for these models is provided by extinction measurements which are both more extensive and more easily interpreted than scattering measurements.

2 Observational determination of α and g

Light scattered by grains is seen in reflection nebulae and as the so-called diffuse galactic light (DGL). The former represents the light from a single cloud while the latter is a superposition of the scattering by many dust clouds of the light from the full stellar population. We shall begin our discussion with the apparently more straightforward case of reflection nebulae.

So far only four reflection nebulae have been successfully observed in the UV: the Merope nebula (Andriesse, Piersma & Witt 1977), the Orion reflection nebula (Witt & Lillie 1978; Morgan, Nandy & Thompson 1982) the inner Orion nebula surrounding the trapezium stars (Mathis *et al.* 1981) and, most recently, NGC 7023 (Witt *et al.* 1982). The values of α and g can be deduced from such observations by developing a model of the nebula and finding the values that yield the closest representation of the observed intensity and colour. The choice of the appropriate model is determined by the geometrical configuration of the nebula. The weakness of this procedure is that both the configuration of the cloud and the location of the illuminating star with respect to it are not known with sufficient reliability. The latter factor plays a particularly crucial role as the following calculation illustrates. We have computed the intensity of scattered light for a crude model of a reflection nebula represented by a plane-parallel optically-thin slab of dust illuminated by a single star. Table 1 demonstrates that in the simplest case (neglecting internal extinction), the same

Table 1. Relation between geometrical configuration and grain chracteristics for a plane-parallel slab of scattering dust producing the same surface brightness.

g	x (pc)		
	D = 0.1 pc	D = 0.4 pc	D = 0.8 pc
0.2	0.25	0.25	0.25
0.3	−0.12	−0.17	−0.19
0.4	−0.17	−0.29	−0.39
0.5	−0.19	−0.37	−0.54
0.6	−0.21	−0.45	−0.67
0.7	−0.23	−0.53	−0.83
0.8	−0.28	−0.63	−1.02

Parameters of the model:

D – lateral distance from the illuminating star;

x – distance from the front boundary of the nebula to the star (negative values indicate positions within or behind the nebula);

T – total thickness of the slab of dust; adopted value: T = 1.0 pc;

θ – angle at which the line of sight crosses the boundary of the nebula; adopted value: $\theta = 90°$.

surface brightness at a given angular distance from the star can be obtained for totally different values of g (using the Henyey–Greenstein scattering function, Henyey & Greenstein 1940) as the star is moved from its initial position in front of the nebula to a location embedded in the slab of dust. The numbers presented in the table are distances of the star from the front surface of the nebula (negative means inside) which result in the same brightness for the particular lateral distance (D) from the star. In general, low values of g (almost isotropic phase function, consequently strong back-scattering) are required when the star is in the foreground, and the phase function can be much more forward peaked when the source of light is contained within the nebula. The inclusion of internal extinction produces a modification in the numbers one obtains, but the qualitative result remains unchanged. The strict equivalence demonstrated in Table 1 holds only for the lines of sight at the same angular distance from the star. The angular dependence of the surface brightness of a reflection nebula can, therefore, be used to determine the geometrical parameters and the scattering characteristics independently (Witt 1977). However, in most cases either the observations do not cover a wide enough range of angular distance from the star or the structure of the nebula is too complicated to be described by a simple geometrical model with an idealized configuration of the scattering cloud, e.g. an infinite slab or a sphere. As the discussion above leads us to expect, all calculations based on the assumption that the illuminating star is in front of the nebula produce relatively low values of g. The determination of α turns out to be even more difficult and in most cases a value of α is assumed based on observations of the DGL.

Most of the observations of reflection nebulae in the ultraviolet have been interpreted with the assumption that the illuminating star is in front of the dust cloud. There are sound observational reasons for questioning this assumption; e.g. in the case of Merope, visual data lead to the requirement that the star should be embedded by approximately 0.35 pc ($\sim$ 0.4 mag extinction) (Greenberg & Roark 1967; Greenberg & Hanner 1970). An independent argument for the presence of dust in front of the star was developed by Jura (1979) who based his conclusions on the evidence for gas in front of the star.

For the extensive reflection nebulosity in Orion, there are several indications that foreground material plays an important role. The stars which illuminate the parts of the nebula with the highest UV brightness are reddened by an $E(B-V)$ of at least 0.06–0.12 mag, which is significantly higher than that of neighbouring stars. At least some of this extinction is therefore local. The structure of the region is probably a result of multiple supernova explosions and is therefore extremely inhomogeneous; as Jura (1979) pointed out, such clumpy structure favours higher values of g. The complicated dynamical history of the region may also give rise to grain properties very far removed from those normally encountered in typical low-density clouds so that the results obtained need not be representative of the average interstellar medium. In both papers where UV observations of the extensive Orion nebula were analysed, the homogeneous infinite slab model was used and gave very low values of g. This result was later totally contradicted by the analysis of more localized reflection in the youngest part of the association surrounding the θ Ori system (Mathis *et al.* 1981). Higher values of g ($\sim$ 0.7) and a value of α levelling off at $\alpha \sim 0.5$ in the FUV tally very well with the numbers one obtains from models discussed in the following section if the deficiency of small grains in the size distribution is taken into account. The inner Orion nebula is a classical case where a size distribution biased towards larger particles is strongly suggested by UV extinction (see Bohlin & Savage 1981).

For NGC 7023, Witt *et al.* (1982), using a spherical model, also arrived at a low value of g (0.25 at 1400 Å). This, however, is a strongly model-dependent result caused mainly by the high FUV surface brightness at large angular distances from the star. The values of g can be

shifted upwards if the spherical model is replaced by one with more material at large angular distances away from the star.

Among other difficulties involved in the analysis of reflection nebulae is the decoupling of the effects of α and g (Witt *et al.* 1982), which causes the uncertainty in one of the two parameters to be reflected in the value obtained for the other.

As has already been mentioned in reference to the Orion cloud, the grains observed in reflection nebulae may not have the same properties as grains present in most low and intermediate-density clouds. Indications of extinction peculiarities less striking than those in Orion exist both for Merope and for NGC 7023 (Witt, Bohlin & Stecher 1981). Whenever this is the case, the results obtained for the nebula cannot be applied to either the diffuse medium or low-density molecular clouds.

The analysis of the DGL measurements is even more difficult than the study of reflection nebulae both in observational techniques and in the interpretation of the data. Observations are usually carried out at low flux levels and have to cover relatively wide fields in order to make the diffuse flux measurable. The final values of the DGL flux are obtained as a result of subtracting the effects of numerous contaminations from the observed flux. Telescopes carried by rockets or low-altitude spacecraft produce observations with a significant air-glow contribution which has to be estimated on the basis of our imperfect understanding of the Earth's upper atmosphere. Other more significant problems remain (e.g. the zodiacal light) even for spacecraft orbiting at higher altitudes. The most difficult problem of all is that of estimating the contribution made by direct starlight. In the visual, extensive stellar photometry makes it possible to estimate relatively accurately the amount of starlight integrated in the telescope aperture. In the UV one has to rely on an uncertain extrapolation of stellar properties measured in the visual and on the careful choice of the fields observed for DGL (Henry *et al.* 1978).

The observations of DGL at high galactic latitudes provide in principle the most straightforward way to measure the asymmetry factor (Sandage 1976; Jura 1979). However, the difficulties in the reduction of the data lead to widely disparate results being obtained depending on the DGL flux 'measured' in each study. When the diffuse flux observed above the galactic plane was relatively high, it was described as being consistent with g as low as 0.25 (Paresce *et al.* 1979). On the other hand, very strong asymmetry ($g \gtrsim 0.9$) was suggested in those studies in which the DGL estimates at high galactic latitudes were low. The difficulties mentioned here are discussed in greater detail by Paresce, McKee & Bowyer (1980) who also derive an intermediate value $g = 0.5$ (together with $\alpha = 0.5$) from their own observations.

The interpretation of measurements closer to the galactic plane is fraught with even greater difficulties since far more sophisticated models are required. A simplified description of the distribution of scattering dust as a plane-parallel slab and the illuminating stars as either homogeneously or exponentially distributed perpendicular to the mid-plane of the Galaxy are assumed. The stellar distribution is a particular problem in the FUV, where most of the light is produced by very young stars scattered in irregular groups and concentrated very strongly towards the galactic plane. The results of the most extensive analysis of DGL measures at low latitudes are given by Witt & Lillie (1978; the observing instrument was the UV telescope on board OAO-2) who derive a rather high value of α (0.6 in the FUV, dropping to 0.3 in the 2200 Å hump) and consistently high values of g throughout the UV (0.6–0.9).

The very confusing image of scattering by grains which emerges from the direct measurements discussed above provides a very strong justification for turning to grain models as sources of more reliable estimates of the scattering properties of interstellar dust. The

increasing number of UV observations has improved our understanding of the interstellar grains, particularly the population of small particles ($a \sim 0.01\ \mu$m), for which the UV extinction curves are the main sources of observational information. In our earlier paper (Greenberg & Chlewicki 1983, hereafter referred to as Paper I) we showed that the constancy of the shape of FUV extinction implies that particles with unsaturated FUV extinction are almost pure absorbers with their average albedo not exceeding an upper limit of ~ 0.2 corresponding to the margin of observational error. This provides an example of the fact that observations of extinction, although not specific enough to enable identification of the composition of grains, can be used to impose restrictions on some of the most important characteristics of grains (sizes, optical constants, etc.). When this approach is followed consistently, it leads to an observationally verifiable model which, without specifying the details of the structure and composition of grains, determines other properties of particles within relatively narrow margins of uncertainty. In the following sections we shall demonstrate the advantage of the model approach over direct measures of the scattering characteristics of grains and apply the results of model calculations to the problem of UV radiative transfer in low-density clouds.

3 Grain models

The model we develop in this paper is intended to provide correct values of α and g at UV wavelengths and the degree of detail in its description of various populations changes according to that requirement. The model is based on the interpretation of extinction curves. Additional constraints, such as cosmic abundance etc. are also taken into account. We ignore polarization in radiative transfer calculations because there is no significant difference between spherical and non-spherical particles in predicting the intensities. In a recent paper (Chlewicki & Greenberg 1984, Paper II) we outlined the basic observational information on grains and the method of its interpretation. The process of developing a model was not followed through in Paper II and only the population of large grains responsible for the visible extinction was discussed in detail. Here we extend that discussion towards a model with sufficient detail to calculate α and g at all UV wavelengths.

In accordance with the conclusions reached in Paper I, we assume that the observed UV extinction is due to three populations of grains differing in size and other properties. The fact that the application of the model is restricted to UV wavelengths makes it possible to simplify the calculations by representing each population with an appropriately chosen single-size grain. The effective size $a_{\rm eff}$ is defined by the following equation:

$$C_{\rm ext}(a_{\rm eff}, \lambda) = K \int C_{\rm ext}(a, \lambda)\, n(a)\, da, \tag{1}$$

where $C_{\rm ext}(a)$ is the extinction cross-section, $n(a)$ represents the size distribution and K is a constant factor. It is immediately obvious that $a_{\rm eff}$ can only be defined within a limited wavelength interval where $C_{\rm ext}$ is represented by the same function of size, independent of wavelength.

$C_{\rm sca}$ leads to a similar definition, although the value of $a_{\rm eff}$ obtained from it is generally different from that in equation (1):

$$C_{\rm sca}(a_{\rm eff}^{\rm (sca)}, \lambda) = K \times \int C_{\rm sca}(a, \lambda)\, n(a)\, da. \tag{1'}$$

The average albedo can be expressed as:

$$\langle \alpha(\lambda) \rangle = \frac{C_{\rm sca}(a_{\rm eff}^{\rm (sca)}, \lambda)}{C_{\rm ext}(a_{\rm eff}, \lambda)}. \tag{2}$$

In our calculations this precise expression was replaced by its obvious approximation:

$$\langle\alpha(\lambda)\rangle = \frac{C_{\rm sca}(a_{\rm eff},\lambda)}{C_{\rm ext}(a_{\rm eff},\lambda)}\,. \qquad (2')$$

The use of equation (2′) instead of (2) may lead to significant errors if applied too generally; for our model, however, direct calculations have confirmed that independent of size distribution the error in the value of $\langle\alpha\rangle$ for either of the two populations contributing to UV scattering is too small to cause a significant change in the values of $\bar{\alpha}$ and $\bar{g}$ as defined in Paper II.

The largest grains in our model, those responsible for the visual extinction, are represented by particles with $a_{\rm eff} = 0.15\ \mu$m. We assume that these particles are inhomogeneous and consist of dielectric cores ($a_{\rm c} = 0.05\ \mu$m) covered with organic refractory mantles (for a justification of such an assumption see Greenberg 1982 and Paper II). $a_{\rm eff} = 0.15\ \mu$m, has been chosen to provide a correct representation of the UV extinction curve for large grains. It is not necessary to use a size distribution which gives a detailed match to the visual extinction because all we require is that the ratio of the magnitude of UV to visual extinction be well approximated. The ratio of UV to visual extinction obtained for an $a = 0.15\ \mu$m particle is close to that calculated for a size distribution of core-mantle particles reproducing correctly both the extinction and the polarization in the visible (Hong & Greenberg 1980). We assume the cores of large grains consist of silicates for which we use the index of refraction of olivine (Huffman & Stapp 1971).

In the UV, the optical properties of the particle are defined by the index of refraction ($m = m' - im''$) of the mantle rather than that of the core which is shielded almost entirely by the absorbing layer of molecular condensate. The optical constants of organic refractory mixtures are not known and we base our estimate on the average properties of complex organic molecules. For the FUV region ($\lambda < 2000$ Å) it is reasonable to assume rather strong absorption (we have adopted $m'' = 0.5$), since all molecules which might occur in such mantles absorb strongly at short wavelengths. The yellow colour of the organic residues indicates that absorption is already present at blue wavelengths which implies that absorption is also present in the near UV (3500–2000 Å). We approximate this by assuming that m'' rises linearly from 0 at 3500 Å to 0.5 at 2000 Å. The resulting extinction curve (after renormalization) is shown as a dotted line in Fig. 1(a). The curve shown in Fig. 1(a) remains valid in the FUV for all particles capable of reproducing the visual extinction independent of their structure whether complex or homogeneous. Such equivalence of all large-particle extinction curves is due to the fact that, with the exception of a few astrophysically irrelevant materials (e.g. MgF), all other solid condensates absorb strongly in the FUV. Consequently, within the range of sizes implied by the visual extinction, the FUV region is always saturated, with $Q_{\rm ext} = C_{\rm ext}/\pi a^2$ slightly in excess of 2.0, $\alpha = 0.5$ and $g = 0.8-0.9$. It turns out that the mixture of dielectric non-absorbing silicate particles and very absorbing graphite particles (Mathis, Rumpl & Nordsieck 1977), when limited to sizes $a > 0.02\ \mu$m (grains contributing to visual extinction), gives a similar trend of α and g in the near UV to that given by the partially-absorbing complex particle we have used for the visual extinction contribution. The difference in the final predictions of both models is due mostly to the small particle contribution.

For the small grains, we assumed that two distinct populations are responsible for the existence of the 2200 Å hump and the FUV rise in extinction (Paper I). The 'FUV' population is represented in our model by silicates with the index of refraction of olivine. Although in general this is not a close representation of the silicate material observed in the interstellar

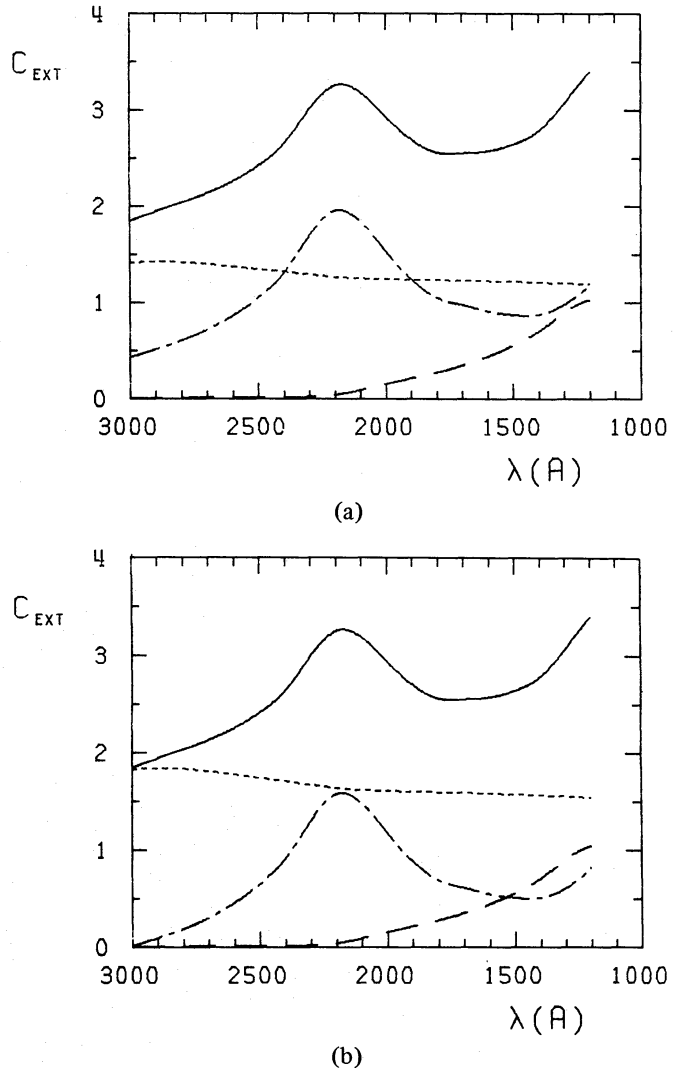

Figure 1. Ultraviolet extinction in a three-population grain model. C_{ext} is normalized to 1 at 5500 Å (the V photometric band). Solid line: the average curve observed in the diffuse medium (see text); dashed line: silicates with the index of refraction of olivine and the effective size of 0.018 μm; dash-dot: the 2200 Å population; dots: core-mantle grains (silicate core, $a_C = 0.05\,\mu$m, organic refractory mantle, $a_M = 0.15\,\mu$m). (a) Core-mantle grains normalized to provide 99 per cent of extinction at 3650 Å (the U band). (b) Core-mantle extinction normalized to 99 per cent at 3000 Å.

medium (the 9.7 μm SiO stretch observed in space is not matched by any terrestrial silicates), the uncertainty in the FUV properties of the silicate component of our model does not significantly affect the final result.

The $\alpha < 0.2$ constraint (< 20 per cent scattering) imposed by the results of Paper I applies to the population of small grains as a whole. For simplicity we assume that only one of the two populations of small grains contributes to scattering; i.e. we let $\alpha = 0$ for the hump population particles. Consequently, for silicates alone α can exceed 0.2 since it is partly offset by $\alpha = 0$ for the other small particle population. In order to cover the whole range of α for small particles allowed by observational uncertainties, we have calculated several models with two populations of silicate grains characterized by $a_{eff} = 0.010\,\mu$m and $a_{eff} = 0.018\,\mu$m.

No commonly adopted explanation has so far been proposed for the 2200 Å hump. Although graphite is considered to be the most likely candidate, it does not explain some of

Table 2. Average scattering parameters of grains for three-population grain models.

λ(Å)	Extinction	Model 1			Model 2			Model 3			Model 4		
		α	g	α_{eq}^{*}	α	g	α_{eq}	α	g	α_{eq}	α	g	α_{eq}
3000	1.84	0.50	0.80	0.407	0.50	0.80	0.407	0.65	0.80	0.546	0.65	0.80	0.546
2800	2.03	0.41	0.82	0.328	0.41	0.82	0.332	0.53	0.82	0.443	0.53	0.82	0.443
2600	2.25	0.32	0.84	0.262	0.32	0.83	0.259	0.41	0.84	0.340	0.42	0.83	0.345
2500	2.41	0.28	0.85	0.232	0.28	0.84	0.299	0.36	0.85	0.298	0.37	0.84	0.303
2400	2.64	0.24	0.85	0.199	0.25	0.84	0.204	0.31	0.85	0.256	0.32	0.84	0.262
2200	3.25	0.18	0.85	0.149	0.19	0.83	0.154	0.23	0.85	0.190	0.24	0.83	0.194
2000	2.94	0.20	0.85	0.165	0.21	0.81	0.166	0.25	0.85	0.207	0.26	0.82	0.208
1800	2.56	0.23	0.85	0.190	0.25	0.80	0.196	0.29	0.86	0.243	0.31	0.81	0.245
1700	2.55	0.23	0.85	0.190	0.25	0.79	0.193	0.30	0.86	0.251	0.32	0.81	0.253
1600	2.57	0.23	0.85	0.190	0.26	0.77	0.197	0.30	0.86	0.251	0.33	0.79	0.255
1500	2.64	0.23	0.85	0.190	0.27	0.75	0.200	0.29	0.85	0.240	0.33	0.77	0.250
1400	2.78	0.22	0.84	0.180	0.27	0.72	0.194	0.28	0.85	0.232	0.33	0.75	0.245
1300	3.07	0.21	0.81	0.166	0.27	0.67	0.185	0.27	0.82	0.216	0.33	0.71	0.235
1200	3.40	0.20	0.76	0.150	0.26	0.64	0.173	0.26	0.79	0.201	0.32	0.68	0.221

* α_{eq} is the value of α to be used with the g=1 approximation in Eq. 20.

the most important observed characteristics of the hump (e.g. the stability of its central wavelength). In our model, we avoid the controversy by assuming that the 2200 Å population contributes all the extinction that remains after subtracting the contributions made by silicates and core-mantle grains from the average interstellar curve. As Fig. 1 demonstrates, the extinction curve obtained for the 2200 Å population resembles that of graphite grains with sizes in the range 0.01–0.02 μm but the agreement is not precise.

Keeping within the observational constraints we have calculated the four models presented in Table 2 and in Figs 1, 2 and 3. Models 1 and 3 have been calculated with 0.010 μm silicates, whereas models 2 and 4 use 0.018 μm silicate grains. We normalize the extinction curves for small grains by assuming that the contribution of the 2200 Å

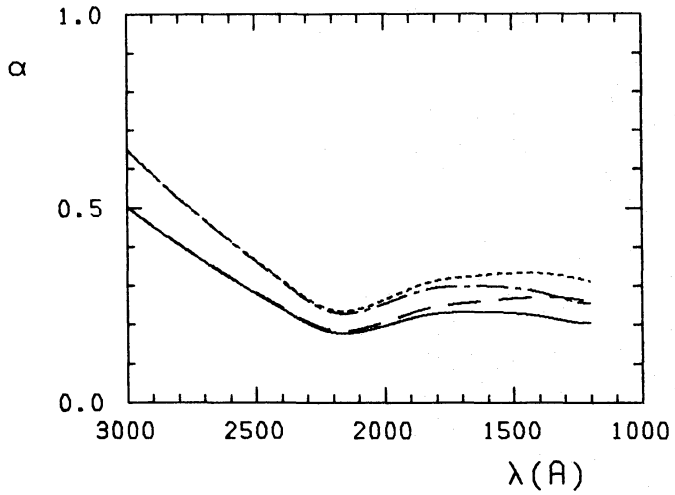

Figure 2. The average albedo at ultraviolet wavelengths for three-population grain models (see Table 2). Solid line: Model 1; dashed line: Model 2; dash-dot: Model 3; dots: Model 4.

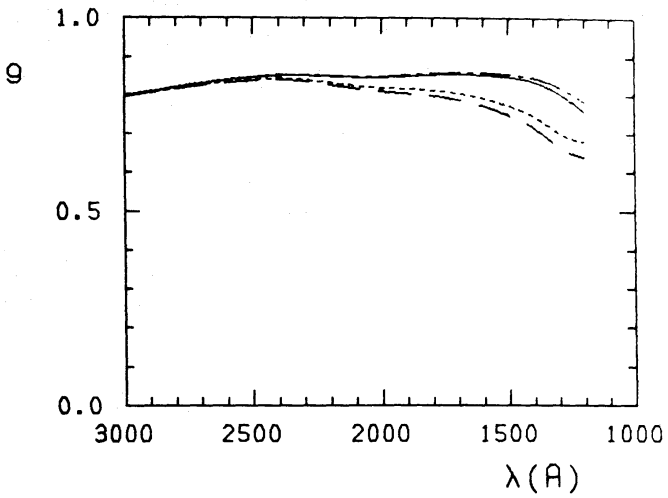

Figure 3. The average asymmetry factor for the same three-population models as in Fig. 2.

population is the same at 1300 and 1700 Å. Two normalizations have been used for the large grain portion of extinction: 'low' (Models 1 and 2) with 99 per cent of extinction at 3650 Å produced by large particles; and 'high' (Models 3 and 4) with 99 per cent contribution at 3000 Å. Since the shape of the visual extinction curve (particularly over the range 5000–3500 Å) is not well represented by our 0.15 μm particles, it is more meaningful to describe the large-particle normalization by their contribution to FUV extinction. The 'low' normalization leads to a ratio of large-grain extinction to the small-grain extinction of $A_L/A_S = 0.65$ at 1300 Å. The 'high' normalization produces a value of $A_L/A_S = 1.02$. As was pointed out in Paper II, these two values are likely to represent the lower and upper limits for the large-grain contribution to FUV extinction in the diffuse interstellar medium. The average interstellar extinction curve which we have used in our calculations has been derived from the data presented in Paper I; within the margin of error it coincides with the average curve of Savage & Mathis (1979).

At this stage, we should like to emphasize only one of the conclusions evident in Table 2; namely, the fact that the values of g remain in the range 0.7–0.9 throughout the UV so that the radiative transfer calculations assuming $g = 1$ are a close approximation to the actual UV penetration into clouds although more precise results may be obtained by appropriately adjusting α (see Section 6).

4 Solutions of the radiative transfer equation

We first summarize briefly the well-known radiative transfer equations to provide ready reference for further discussion and, in particular, to provide a clear basis for some analytical and empirical results.

The solution of the equation of radiative transfer depends strongly on the geometrical configuration of the cloud. We shall limit our consideration to plane-parallel and spherical clouds for both of which results are obtained relatively easily.

In a plane-parallel cloud, the transfer of radiation is governed by the equation

$$\mu \frac{\partial I(r,\mu)}{\partial r} = -\kappa(r)[I(r,\mu) - S(r,\mu)] \tag{3}$$

where $I(r, \mu)$ is the specific intensity at the coordinates r, μ; r is measured from the centre of the cloud and the angle $\theta = \arccos\mu$ is measured with respect to the direction of

increasing r; S is the source function, and κ is the volume absorption coefficient. If S arises only from scattering (no emission) it takes the form:

$$S(r,\mu) = \frac{\alpha}{4\pi} \int p\,(\cos\theta')\, I(r,\mu')\, d\Omega'. \tag{4}$$

In equation (4) p is the scattering phase function and θ' is the angle between the incident and scattered beam. The assumption that the phase function is independent of azimuthal angle (cylindrically symmetric scattering) allows us to rewrite equation (4) as

$$S(r,\mu) = \frac{\alpha}{2} \int_{-1}^{+1} p\,(\cos\theta')\, I(r,\mu')\, d(\cos\theta'). \tag{5}$$

With the differential optical depth defined as

$$d\tau = -\kappa(r)\, dr, \tag{6}$$

equation (3) finally becomes

$$\mu \frac{\partial I(\tau,\mu)}{\partial \tau} = I(\tau,\mu) - S(\tau,\mu). \tag{7}$$

Equation (7) can be applied equally to homogeneous $[\kappa(r) = \kappa_0]$ and inhomogeneous $[\kappa = \kappa(r)]$ clouds in the plane-parallel geometry because inhomogeneity does not affect the angular distribution of radiation. This is not the case in a spherical cloud for which the radiative transfer equation assumes the more complicated form:

$$\mu \frac{\partial \tau}{\partial r} - \frac{1-\mu^2}{r} \frac{\partial I}{\partial \mu} = \kappa (I - S). \tag{8}$$

If the cloud is homogeneous the optical depth can be defined as

$$\tau_c = \kappa R, \qquad \tau(r) = \kappa (R - r) \equiv \tau \tag{9}$$

where R is the cloud radius and τ_c is the optical depth at the centre of the cloud.

In most applications of radiative transfer calculations, the angular dependence of the radiation is not important and may be removed from the final solution by introducing the average intensity, J:

$$J(\tau) = \frac{1}{4\pi} \int I(\tau, \cos\theta)\, d\Omega. \tag{10}$$

4.1 SOLUTION FOR $g \neq 1$

In all 'exact' calculations presented in this paper we use the spherical harmonics method developed by Flannery, Roberge & Rybicki (1980). The method is based on the expansion of the phase function and the specific intensity in series of Legendre polynomials. The τ-dependent coefficients of that expansion for the specific intensity are determined from an infinite system of differential equations into which the equation of radiative transfer is transformed. A finite approximation is obtained by truncating the series expansion to an even number of terms, $L = 2M$. Flannery, Roberge & Rybicki described the solution of the radiative transfer equation for plane-parallel and homogeneous spherical clouds and found

that the decay of individual terms in the Legendre expansion of the specific intensity with optical depth is expressed by exponentials for the plane-parallel geometry or, for spherical clouds, by spherical Bessel functions of the variable $k_i\tau (i = 1, \ldots, M)$. The coefficients k_i are calculated from the solution of the eigenvalue problem for a matrix determined by the value of α and the Legendre expansion coefficients for the phase function. The amplitudes of various terms in the angular expansion of the specific intensity are determined by the intensity at the boundary and the boundary conditions are ultimately reduced to a matrix equation of order M. In most cases, the spherical harmonics method leads to a very accurate solution for the average intensity J with even relatively low values of M ($M = 12$ has been sufficient to obtain a 10^{-4} accuracy in all calculations presented in this paper). A finite solution becomes difficult to obtain for low values of α and for values of g close to 1 when the angular dependence of the specific intensity cannot be represented accurately by a finite Legendre expansion. For the plane-parallel configuration, the computations using the spherical harmonics method are straightforward and fast, although efficient algorithms for the eigenvalue problem and the matrix equation are required. For the spherical geometry, the numerical solution becomes difficult and sometimes impossible for certain sets of α, g and τ_c for which the boundary condition matrix is so ill-conditioned that the amplitudes of the Legendre expansion terms cannot be calculated. Such difficulties are particularly likely to occur for low values of τ_c ($\tau_c < 10$) accompanied by high values of g ($g > 0.5$) (*cf.* Bell & Williams 1983). As a result, the application of the spherical harmonics method to low-density clouds in spherical geometry is somewhat limited.

4.2 SOLUTION FOR $g = 1$

If $g = 1$, the source function is particularly simple:

$$S(\tau, \mu) = \alpha I(\tau, \mu). \tag{11}$$

For the plane-parallel configuration, the radiative transfer equation is reduced to

$$\mu \frac{\partial I(\tau, \mu)}{\partial \tau} = (1 - \alpha) I(\tau, \mu). \tag{12}$$

The solution of equation (12) is obvious and leads to the following formula for the average intensity:

$$J(\tau) = \frac{1}{2} I_0 \{E_2 [(1 - \alpha)\tau] + E_2 [(1 - \alpha)(2\tau_c - \tau)]\}. \tag{13}$$

We have assumed here that the intensity of the incoming radiation is isotropic at both boundaries of the clouds, i.e. $I(\mu) = I_0$. In equation (13), E_2 denotes the second exponential integral, defined by

$$E_2(z) = \int_1^\infty \frac{\exp(-zt)}{t^2} dt. \tag{14}$$

Each term in equation (13) represents radiation passing through one of the two boundaries of the cloud.

In a spherical cloud, for $g = 1$, equation (8) is transformed into:

$$\mu \frac{\partial I}{\partial r} + \frac{1 - \mu^2}{r} \frac{\partial I}{\partial \mu} = \kappa (1 - \alpha) I. \tag{15}$$

If the cloud is homogeneous, the solution only requires some trigonometric transformations, which lead to:

$$J(\tau) = \frac{1}{2} I_0 \int_0^1 \exp\left[-(k_1^2 + k_2^2 \mu^2)^{1/2}\right][\exp(k_2 \mu) + \exp(-k_2 \mu)]\, d\mu. \tag{16}$$

In order to simplify the notation we have introduced the following symbols:

$$\begin{aligned} k_1^2 &= [\tau_c^2 - (\tau_c - \tau)^2](1-\alpha)^2 \\ k_2 &= (\tau_c - \tau)(1-\alpha). \end{aligned} \tag{17}$$

Although the form of equation (16) is not intuitively obvious, its validity may easily be confirmed in two limiting cases: $\tau = 0$ and $\tau = \tau_c$. If $\tau = 0$, then $k_1 = 0$, $k_2 = \tau_c(1-\alpha)$ and $J(0)$ becomes:

$$J(0) = \frac{1}{2} I_0 + \frac{1}{2} I_0 \frac{1 - \exp[-2\tau_c(1-\alpha)]}{2\tau_c(1-\alpha)}. \tag{18}$$

It is easy to prove by direct integration that the second term correctly represents radiation passing through the cloud with the degree of attenuation determined by the total optical depth, $2\tau_c$. As expected, $J \to I_0$ when $\tau_c \to 0$ and $J \to (1/2)I_0$ when $\tau_c \to \infty$. If $\tau = \tau_c$, then $k_1 = \tau_c(1-\alpha)$, $k_2 = 0$ and equation (16) yields:

$$J(\tau_c) = I_0 \exp[-\tau_c(1-\alpha)]. \tag{19}$$

The solution of equation (15) described above can be generalized to incorporate inhomogeneous clouds although the form of $J(\tau)$ will depend on the way in which optical density changes within the cloud and in most cases the simplicity of equation (16) will be lost.

5 UV intensities in clouds

We have emphasized in Section 3 that the large-grain contribution to UV extinction (A_L/A_S) is restricted by observations to a relatively narrow range. The maximum effects on α and g of existing uncertainties in the value of A_L/A_S can be estimated by comparing either Models 1 and 3 or Models 2 and 4 in Table 2. With the large-grain contribution approximately fixed, a significant increase in the average value of α for a given model can only be achieved by adopting increased sizes of small grains. Since small particles scatter almost isotropically, their increased contribution to scattering makes the average phase function more isotropic (lower value of g). As a result, realistic grain models with a high value of α must have a value of g lower than those in Table 2. More isotropic scattering reduces the UV penetration and partly offsets the effects of increased albedo. Consequently, the differences in UV penetration predicted by various models are smaller than might be expected. The tendency for α and g to change in an opposite (compensating) way when the adopted sizes of small grains are modified, can be seen from the comparison of Models 1 and 2 (low A_L/A_S) or Models 3 and 4 (high A_L/A_S) in Table 2. The effect of $\alpha - g$ compensation is well illustrated by Figs 4 and 5. Fig. 4 compares the two extreme models in the set presented in Table 2 (Model 1 and Model 4) with the graphite + silicate model of Mathis *et al.* (the values of α and g come from White 1979) and with the extrapolation of observational DGL results derived as Model 2 in Roberge, Dalgarno & Flannery (1981).

So far we have only discussed the influence on the average values of α and g produced by changes in grain sizes adopted for various grain models. It is obvious that similar effects can

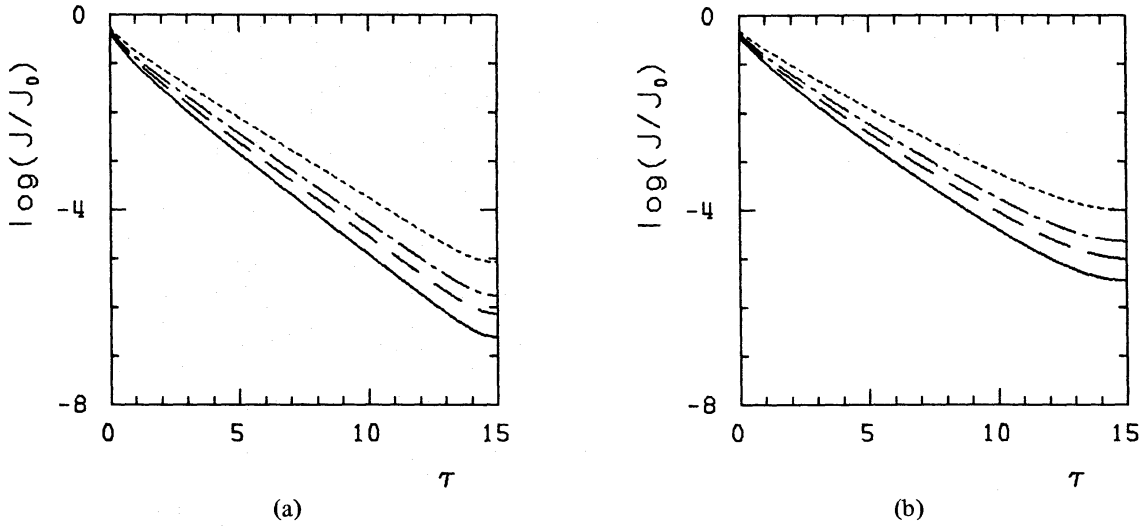

Figure 4. The penetration of UV radiation at 1300 Å in a cloud with central optical depth $\tau_c = 15$. Solid line: Model 1 according to Table 2 ($\alpha = 0.21$, $g = 0.81$); dashed line: Model 4 according to Table 2 ($\alpha = 0.33$, $g = 0.71$); dash-dot: graphite + silicate model of Mathis *et al.* (1977) ($\alpha = 0.43$, $g = 0.63$); dots: Model 2 of Roberge *et al.* (1981) ($\alpha = 0.6$, $g = 0.5$). (a) Plane-parallel configuration, (b) spherical configuration.

also occur when sizes of particles change as a result of growth or destruction under conditions different from those in the diffuse medium (molecular clouds, regions affected by shocks). However, physical changes in grain characteristics are also likely to change the value of A_L/A_S and thus may not produce an $\alpha - g$ compensation. A full discussion of scattering models which can be applied to dense molecular clouds (grain growth) and to regions affected by star formation (particle erosion by shock waves and radiation) will be included in a separate paper.

In Figs 4 and 5 the decay of the average intensity is presented down to the optical depth of 15, for which the FUV intensity drops below 10^{-4} of the diffuse background outside. We

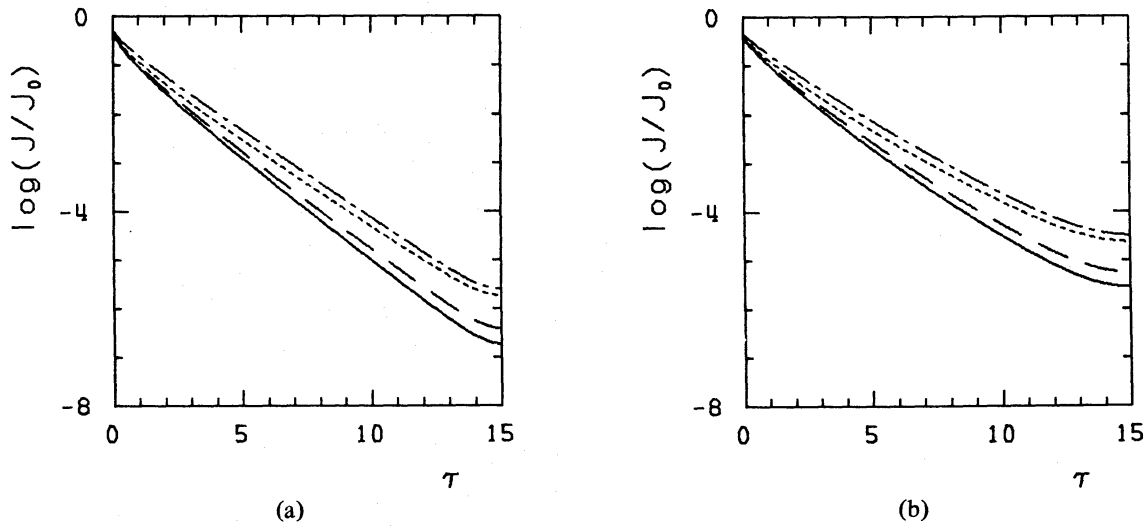

Figure 5. The UV penetration for the same models as in Fig. 4 calculated at $\lambda = 2200$ Å. Solid line: Model 1 ($\alpha = 0.18$, $g = 0.88$); dashed line: Model 4 ($\alpha = 0.24$, $g = 0.83$); dash-dot: Mathis *et al.* (1977) ($\alpha = 0.52$, $g = 0.48$); dots: Roberge *et al.* (1981) ($\alpha = 0.33$, $g = 0.89$). (a) Plane-parallel geometry, (b) spherical geometry.

assume that in most clouds with the central optical depth $\tau_c \geqslant 15$ at 1300 Å (corresponding to $A_V = 5$ mag), the density is high enough for most hydrogen to be in molecular form so that H_2 fluorescence is likely to prevent the intensity of radiation in the cloud from falling significantly below the values shown in Fig. 4. For diffuse clouds, where H_2 fluorescence cannot occur, radiation below $10^{-4}-10^{-5}$ of the normal DGL intensity is unlikely to play a significant role in their evolution. The intensity of radiation at optical depths higher than 15 is therefore relatively unimportant in most applications.

Because of the $\alpha - g$ compensation in the UV penetration the Mathis *et al.* model, although based on entirely different assumptions about the properties of grains, leads to FUV penetration higher by only a factor of 2 than our Model 4. The differences between these models are more pronounced at $\lambda = 2200$ Å. The fact that in the Mathis *et al.* model graphite particles responsible for the existence of the 2200 Å hump are relatively large ($\langle a \rangle \sim 0.02\,\mu$m) produces a very high average albedo in the hump which in turn results in the relatively slow decay of intensity (Fig. 5).

The large variety of observational results makes it impossible to compare them with theoretical models in a systematic way. As a result of $\alpha - g$ compensation many of the observed pairs $[\alpha, g]$, which are unacceptable from the point of view of grain properties (Paper II), may lead to UV intensities close to those predicted by physically consistent models. The values $\alpha_{1400} = 0.6$ and $g_{1400} = 0.25$ derived by Witt *et al.* (1983) from observations of the planetary nebula NGC 7023 may be taken as an example. At 1400 Å such values of $\bar{\alpha}$ and $\bar{g}$ cannot be matched by *any* grain model with a realistic large-grain contribution (*cf.* Paper II). The intensities obtained for $\alpha = 0.6$ and $g = 0.25$ are, however, only slightly larger than those of Model 4 and are roughly consistent with the Mathis *et al.* model. The UV penetration in clouds cannot therefore serve as a reliable test of the validity of direct measures of α and g. Such test is provided instead by the consistency of the grain properties implied by the values of α and g derived from direct measures of scattered light with the same properties obtained from other more reliable observations (a convenient way of assessing such consistency was proposed in Paper II).

6 The $g = 1$ approximation

The fact, emphasized in Section 2, that for all our grain models the values of g are relatively high ($g \approx 0.7-0.9$) raises the possibility of replacing the exact solution of the radiative transfer equation for the given g and α with that for $g = 1$ and an appropriately chosen value of $\alpha_{eq} = \alpha_{eq}(\alpha, g)$. The $g = 1$ solution requires no sophisticated numerical algorithms even at the rather limited level necessary for the spherical harmonics method and does not pose the numerical difficulties which may appear in the exact solution for spherical clouds. Its particular advantage is for complete radiative transfer models covering a range of wavelengths for the same optical depth. The most time-consuming part of the spherical harmonics algorithm is the calculation of matrix eigenvalues, which depend on the values of α and g and therefore their evaluation has to be repeated for every wavelength covered by the model. The $g = 1$ solution is in such cases much faster and can be calculated even on a small computer.

Since the rate of decay of the average intensity with optical depth depends on both α and g, it is impossible to find α_{eq} satisfying the condition $J(\tau, \alpha, g) = J(\tau, \alpha_{eq}, g = 1)$ for all values of τ. We demand therefore that the algorithm for the derivation of α_{eq} should provide the closest match at $\tau = 15$. As will be demonstrated below, this requirement guarantees a good approximation of the exact solution over a range of τ from 0 to more than 20. By studying the behaviour of $J(\tau = 15)$ as a function of α and g we have found

the following heuristic algorithm for calculating α_{eq}:

$$\alpha_{eq} = \alpha + (1 - g)\, h, \tag{20}$$

where

$$h = \begin{cases} h_0 & \text{for } h_0 \geqslant -0.425 \\ 0.339\, h_0 - 0.281 & \text{for } h_0 < -0.425 \end{cases}$$

and

$$h_0 = \alpha/(g - 1.712). \tag{22}$$

Figs 6, 7 and 8 demonstrate that replacing the exact solution $J(\tau, \alpha, g)$ with $J(\tau, \alpha_{eq}, g = 1)$ produces an excellent match at $\tau = 15$ for a wide range of both α and g. Since the difference between the exact and approximate solutions does not depend strongly on the value of τ_c the results for $\tau_c = 15$ presented in Figs 6, 7 and 8 remain valid even for clouds with a very high central optical depth. For $g > 0.7$ and $\alpha < 0.4$ the accuracy of the approximation at $\tau = 15$ remains within 6 per cent. Figs 7 and 8 show that even for g as low as 0.5 and a high value of α, $\alpha = 0.6$, the accuracy at $\tau = 15$ is only slightly worse than 10 per cent. The $g = 1$ solution, which correctly reproduces the intensity at $\tau = 15$, does not match the decay rate of the exact solution. As a result, the amount of radiation is underestimated for $\tau < 15$ (the influence of reduced α) and overestimated for $\tau > 15$ where the effects of the forward-throwing phase function dominate the transfer of radiation. However, in the range $g > 0.7$, $\alpha < 0.4$, the error for all values of $\tau \leqslant 20$ does not exceed 10 per cent. The closeness of the approximation deteriorates rapidly with decreasing g and increasing α, but the deviation remains within a factor of 2 for $\alpha = 0.6$ and g as small as $g = 0.5$ [Figs 7(b) and 9(b)]. At low optical depths the approximation can be improved considerably by reducing the value of h in equation (20). In order to improve the match by a factor of 2 it is sufficient to change

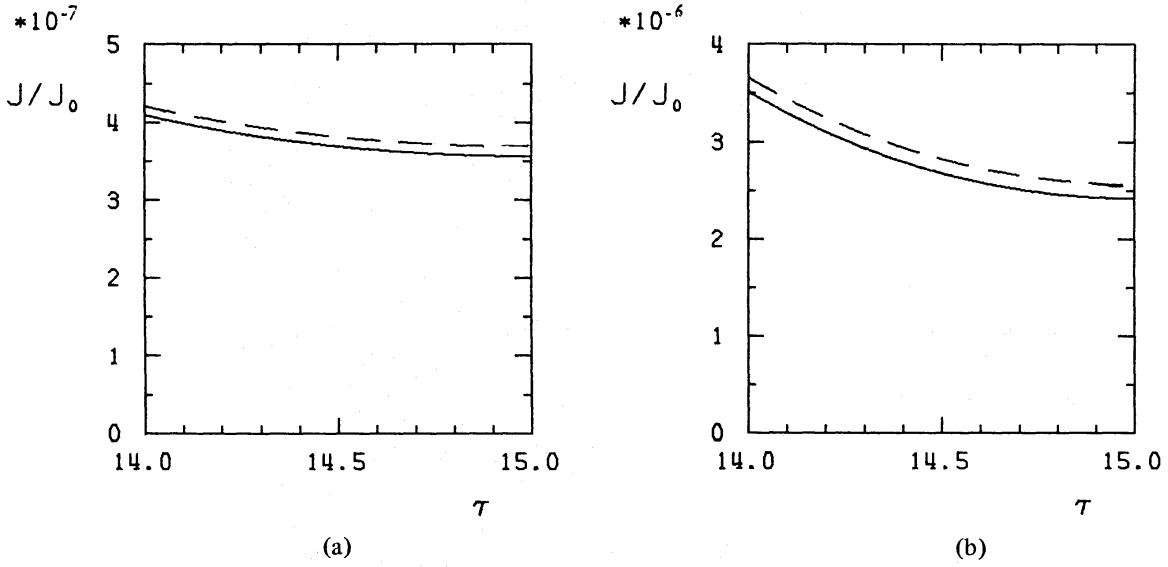

Figure 6. The $g = 1$ approximate solution of the radiative transfer equation for $\alpha = 0.21$, $g = 0.81$ and $\tau_c = 15$. Solid line: the exact solution (the spherical harmonics algorithm with the accuracy of $\sim 10^{-4}$); dashed line: the $g = 1$ approximation. (a) Plane-parallel geometry, (b) spherical geometry.

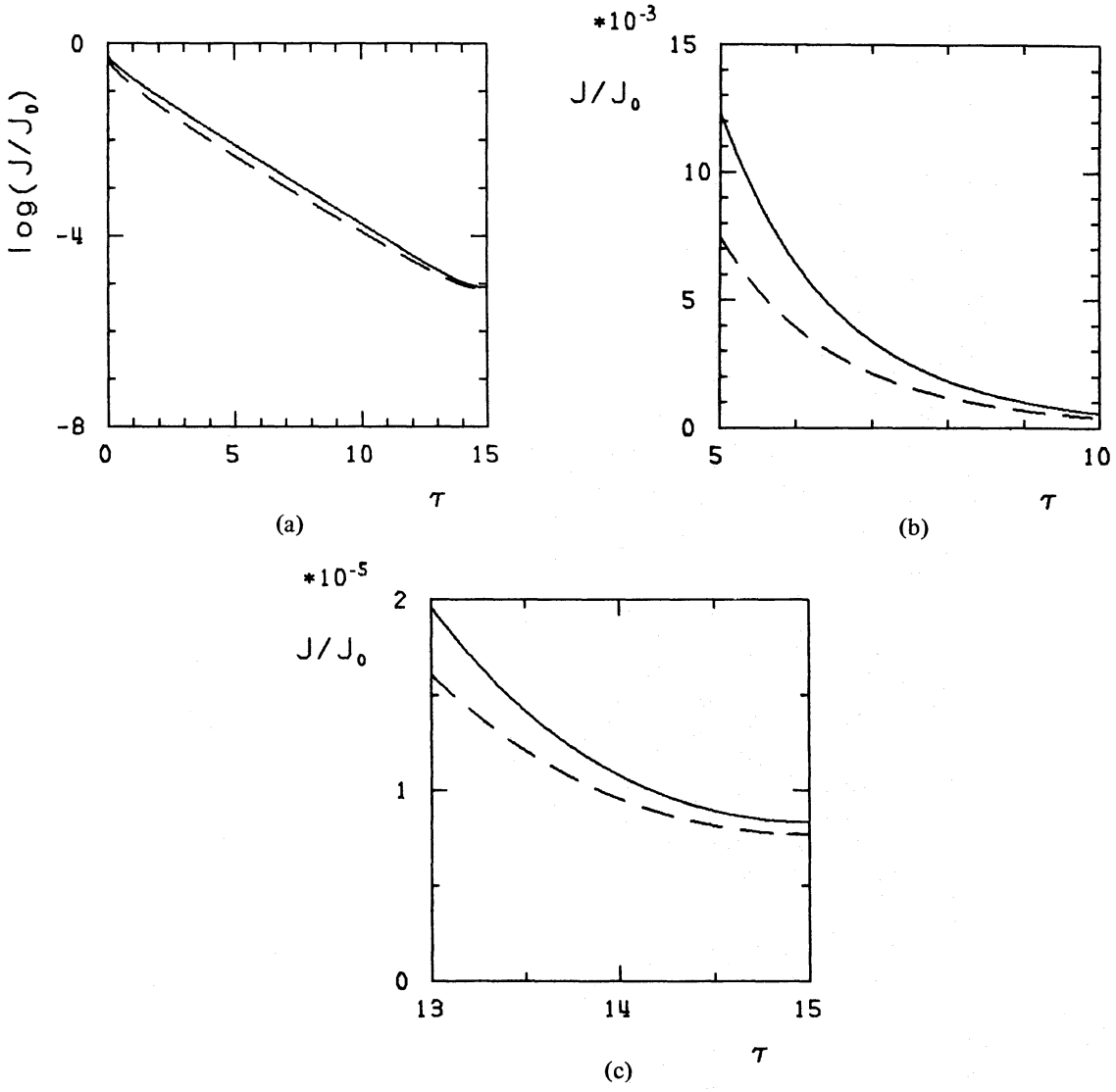

Figure 7. The $g = 1$ approximation for a plane-parallel cloud with $\alpha = 0.6$, $g = 0.5$ and $\tau_c = 15$. Solid line: the exact solution; dashed line: the $g = 1$ approximation. (a) The complete solutions presented as $\log(J)$ versus τ for $0 < \tau < 15$. (b) The same solutions presented as J versus τ for $5 < \tau < 10$ (the largest error of approximation). (c) The same as (b) for the range $13 < \tau < 15$ (the smallest error).

the value of h derived from equation (21) by 10 per cent for $\tau = 10$ and by 20 per cent for $\tau = 5$.

The accuracy of radiative transfer solutions required in the models of the dynamics and chemistry of molecular and diffuse clouds is relatively low because of the enormous uncertainties involved in the determination of other parameters controlling the physical processes in the interstellar medium. The approximation provided by the $g = 1$ solution is therefore sufficiently close not only for grain scattering models presented in Table 2 but also for grain populations with more isotropic average phase functions similar to the Mathis *et al.* model. Since in molecular clouds, both the sizes of large grains and their contribution to the total extinction and scattering are likely to be increased, we expect the values of g to be higher than in the diffuse medium. The $g = 1$ approximation is therefore even more reliable in application to molecular clouds than to the diffuse medium. Because of its simplicity, the approximate solution of the radiative transfer problem makes it possible to test the effect

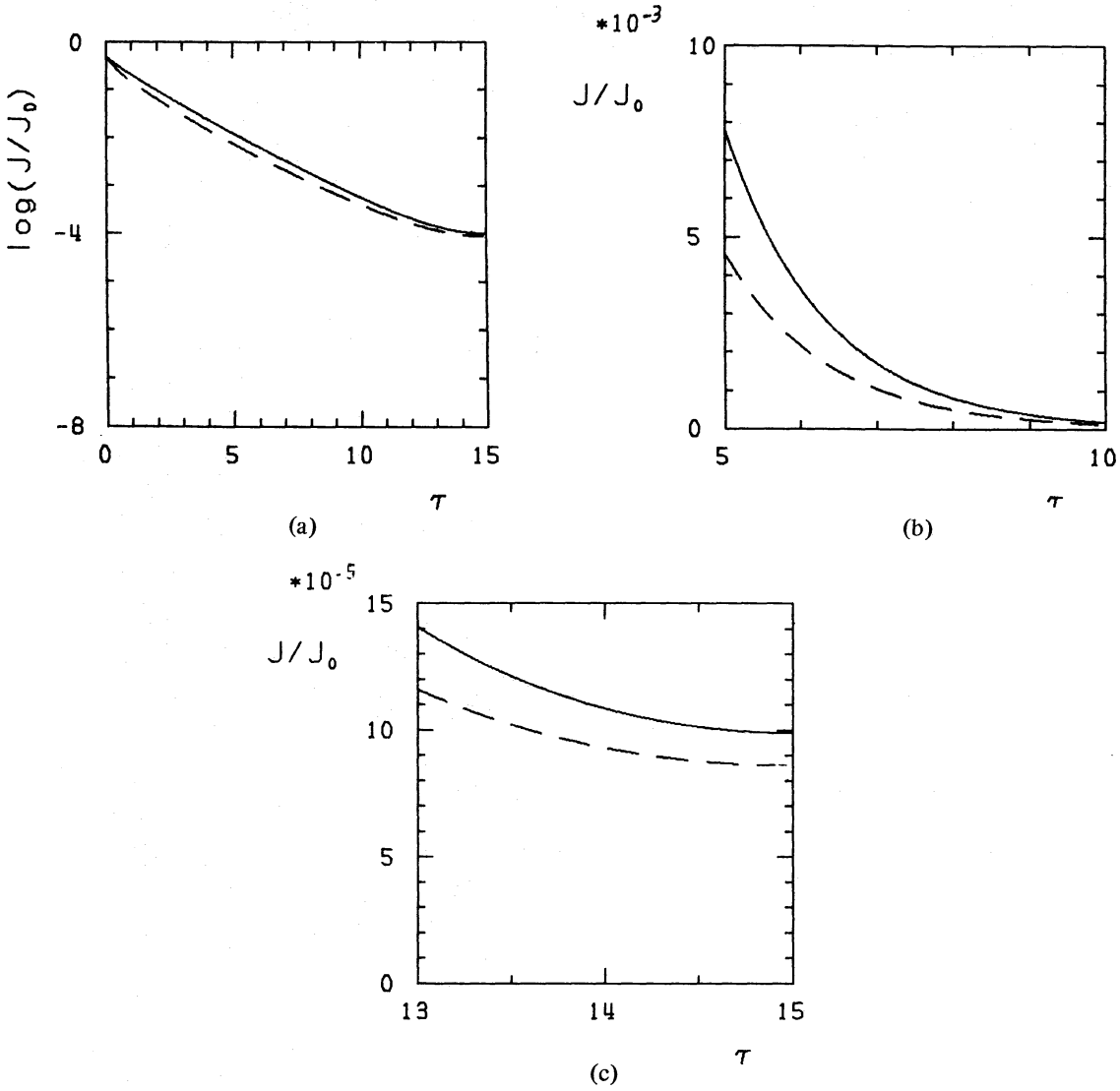

Figure 8. The same as Fig. 7 for a spherical cloud.

of many different grain models on the structure and evolution of clouds. It can also be easily generalized to incorporate geometrical configurations other than a plane-parallel slab and a homogeneous sphere since, as Figs 6, 7 and 8 demonstrate, the closeness of the approximation does not depend on the geometry of the cloud.

7 Conclusions

We have shown that the general optical properties of interstellar grains in the ultraviolet are more reliably deduced from the wavelength dependence of extinction than from measures of reflection nebulae and the diffuse galactic light. The predicted values of the albedo in the ultraviolet are found to be $0.2 \lesssim \alpha \lesssim 0.35$ with a dip towards the lower values in the 2200 Å hump and a rise beyond $\alpha = 0.35$ for $\lambda > 2600$ Å. The predicted values of g are $0.85 \gtrsim g \gtrsim 0.7$ and are relatively insensitive to wavelength for $\lambda \leqslant 3000$ Å.

The discrepancy between the the low values of g derived from reflection nebulae and the high ones we predict can be explained as due to the assumption that the illuminating star is not embedded in the nebulosity.

The radiative transfer results do not depend strongly on the choice of grain models because of the tendency for an increase in α to be accompanied by a decrease in g and vice versa.

The fact that g is close to unity over a significant wavelength range makes it possible to develop a very accurate approximation for radiative transfer based on the trivially simple solution for $g = 1$.

Acknowledgment

We are grateful to C. E. P. M. van de Bult for providing us with his elegant computer codes for Mie theory calculations.

References

Andriesse, C. D., Piersma, Th. R. & Witt, A. N., 1977. *Astr. Astrophys.*, **54,** 841.
Bell, K. L. & Williams, D. A., 1983. *Mon. Not. R. astr. Soc.*, **202,** 407.
Bohlin, R. C. & Savage, B. D., 1981. *Astrophys. J.*, **249,** 109.
Chlewicki, G. & Greenberg, J. M., 1984. *Mon. Not. R. astr. Soc.* **210,** 791.
Cowie, L. L., Songaila, A. & York, D. G., 1979. *Astrophys. J.*, **230,** 469.
Flannery, B. P., Roberge, W. & Rybicki, G., 1980. *Astrophys. J.*, **236,** 598.
Greenberg, J. M., 1978. *Cosmic Dust,* p. 187, ed. McDonnell, J. A. M., Wiley.
Greenberg, J. M., 1982. *Submillimetre Wave Astronomy*, p. 261, eds Beckman, J. E. & Phillips, J. P., Cambridge University Press.
Greenberg, J. M. & Chlewicki, G., 1983. *Astrophys. J.*, **272,** 563.
Greenberg, J. M. & Hanner, M. S., 1970. *Astrophys. J.*, **161,** 997.
Greenberg, J. M. & Roark, T., 1967. *Astrophys. J.*, **147,** 917.
Greenberg, J. M., van de Bult, C. E. P. & Allamandola, L. J., 1983. *J. Phys. Chem.*, **87,** 4243.
Henry, R. C., Anderson, R., Feldman, P. D. & Pastie, W. G., 1978. *Astrophys. J.*, **222,** 902.
Henyey, L. G. & Greenstein, J. L., 1940. *Astrophys. J.*, **93,** 70.
Hong, S. S. & Greenberg, J. M., 1980. *Astr. Astrophys.*, **88,** 194.
Huffman, D. R. & Stapp, J. L., 1971. *Nature Phys. Sci.*, **229,** 45.
Jura, M., 1979. *Astrophys. J.*, **231,** 732.
Lillie, C. F. & Witt, A. N., 1976. *Astrophys. J.*, **208,** 64.
Mathis, J. S., Perinotto, M., Patriarchi, P. & Schiffer, F. H., 1981. *Astrophys. J.*, **249,** 99.
Mathis, J. S., Rumpl, W., & Nordsieck, K. H., 1977. *Astrophys. J.*, **217,** 425.
Morgan, D. H., Nandy, K. & Thompson, G. I., 1982. *Mon. Not. R. astr. Soc.*, **199,** 399.
Paresce, F., McKee, C. F. & Bowyer, S., 1980. *Astrophys. J.*, **240,** 387.
Paresce, F., Margon, B., Bowyer, S. & Lampton, M., 1979. *Astrophys. J.*, **230,** 304.
Prasad, S. S. & Tarafdar, S. P., 1983. *Astrophys. J.*, **267,** 603.
Roberge, W. D., Dalgarno, A. & Flannery, B. P., 1981. *Astrophys. J.*, **243,** 817.
Sandage, A., 1976. *Astr. J.*, **81,** 954.
Savage, B. D. & Mathis, J. S., 1979. *Ann. Rev. Astr. Astrophys.*, **17,** 73.
Shah, G. A. & Krishna Swamy, K. S., 1978. *Kodaikanal Obs. Bull., Ser. A,* **2,** 95.
Taft, E. A. & Phillip, H. R., 1965. *Phys. Rev.*, **138,** A187.
Tosatti, B. & Bassani, F., 1970. *Il Nuovo Cimento,* **65B,** 161.
White, R. L., 1979. *Astrophys. J.*, **229,** 954.
Witt, A. N., 1977. *Astrophys. J. Suppl.*, **35,** 1.
Witt, A. N. & Lillie, C. F., 1978. *Astrophys. J.*, **222,** 909.
Witt, A. N., Bohlin, R. C. & Stecher, T. P., 1981. *Astrophys. J.*, **244,** 199.
Witt, A. N., Walker, G. A. H., Bohlin, R. C. & Stecher, T. P., 1982. *Astrophys. J.*, **261,** 492.